Research
A SCIENCE PARTNER JOURNAL

RESEARCH ARTICLE

Efficient Red Electroluminescent Copper Complexes with Fluorination-Balanced Dual Emission

Xinjing Lou[1], Gang Chen[1], Chunyu Liu[1], Jing Zhang[1*], Jiexu He[1], Jixiu Niu[1], Chunbo Duan[1], Chunmiao Han[1], Andrey A. Karasik[2], and Hui Xu[1*]

[1]Key Laboratory of Functional Inorganic Material Chemistry (Ministry of Education), School of Chemistry and Material Science, Heilongjiang University, Harbin 150080, P. R. China. [2]Arbuzov Institute of Organic and Physical Chemistry, FRC Kazan Scientific Center, Russian Academy of Sciences, Kazan 420088, Russian Federation.

*Address correspondence to: zhangjing@hlju.edu.cn (J.Z.); hxu@hlju.edu.cn (H.X.)

Citation: Lou X, Chen G, Liu C, Zhang J, He J, Niu J, Duan C, Han C, Karasik AA, Xu H. Efficient Red Electroluminescent Copper Complexes with Fluorination-Balanced Dual Emission. *Research* 2026;9:Article 1088. https://doi.org/10.34133/research.1088

Submitted 28 October 2025
Revised 11 December 2025
Accepted 19 December 2025
Published 14 January 2026

Copyright © 2026 Xinjing Lou et al. Exclusive licensee Science and Technology Review Publishing House. No claim to original U.S. Government Works. Distributed under a Creative Commons Attribution License (CC BY 4.0).

Copper complexes hold a promise for electroluminescent applications, owing to their dual emissive feature based on the moderate spin-orbital coupling effect of Cu^+ ion for controllable singlet–triplet conversion. However, efficient red dual emission from copper complexes remains an important challenge, because emission wavelengths and thermally activated delayed fluorescence (TADF)/phosphorescence (PH) ratios are simultaneously correlated to electronic effects. Herein, fluorine atoms with suitable electron-withdrawing inductive effect were introduced into a typical tridentate phosphine ligand coordinated CuI skeleton, namely, TTPPCuI, to reduce the lowest unoccupied molecular orbital (LUMO) energy levels, giving rise to narrowed energy gaps between the highest occupied molecular orbital and LUMO, corresponding to emission wavelengths red shifted from 574 to 603 nm. Fluorine atoms simultaneously enhance metal-ligand charge transfer, therefore adjusting positive and reverse intersystem crossing for dual emission balance, leading to TADF/PH ratios changing from 56/44 over 75/25 to 83/17. The devices based on these fluorinated CuI complexes realized efficient red electroluminescence with the maximum wavelength and external quantum efficiency beyond 600 nm and 20%, respectively. These results demonstrate that, based on electronic effects from functional groups, ligand engineering is a feasible way for comprehensively manipulating excited-state characteristics of dual-emissive copper complexes.

Introduction

Organic light-emitting diodes (OLEDs) are widely applied in modern display and lighting technologies due to their self-luminescence, wide color gamut, low power consumption, and flexible processability [1–7]. They have also demonstrated considerable potential in wearable devices [8], flexible electronics [9,10], and emerging optoelectronic applications [11]. Enhancing exciton utilization efficiency (EUE) is a key strategy for improving OLED performance [12]. According to spin statistics [13], singlet and triplet excitons are generated in a 1:3 ratio during electrical excitation. In conventional fluorescence (FL) [14], phosphorescence (PH) [15], and thermally activated delayed fluorescence (TADF) [16], either the first singlet (S_1) or triplet (T_1) excited state contributes to emission through a single radiative transition process (Fig. 1A). These mono-emissive pathways tend to cause exciton accumulation, which intensifies singlet–triplet and triplet–triplet annihilation (STA [17] and TTA [18], respectively). To address these limitations, dual-emissive materials that combine TADF and PH have emerged as a promising solution (Fig. 1A). These materials offer direct radiative channels for both singlet and triplet excitons, reducing energy loss and facilitating efficient exciton management by accelerating emission and suppressing quenching processes [19–27].

Among dual-emissive systems, copper complexes stand out due to their moderate spin-orbit coupling (SOC) and tunable excited-state properties [20,28], including metal-to-ligand charge transfer (MLCT), iodine-to-ligand charge transfer (ILCT), and intraligand charge transfer (LCT) states [29,30]. Moderate SOC allows both reverse intersystem crossing (RISC) from the T_1 to the S_1 and radiative decay from the T_1 to the ground state (S_0), enabling dual emission without reliance on heavy metals [31–33]. Fine-tuning the electronic effects, steric hindrance, and charge distribution of ligands enables control over excited-state energy levels and transition pathways, allowing a balanced contribution from TADF and PH. However, TADF and PH are inherently competitive. Enhancing MLCT can improve triplet localization and promote PH [20], but simultaneously narrows the singlet–triplet splitting energy (ΔE_{ST}), which promotes RISC and enhances TADF [34]. Moreover, MLCT modulation alters the structure of excited-state energy

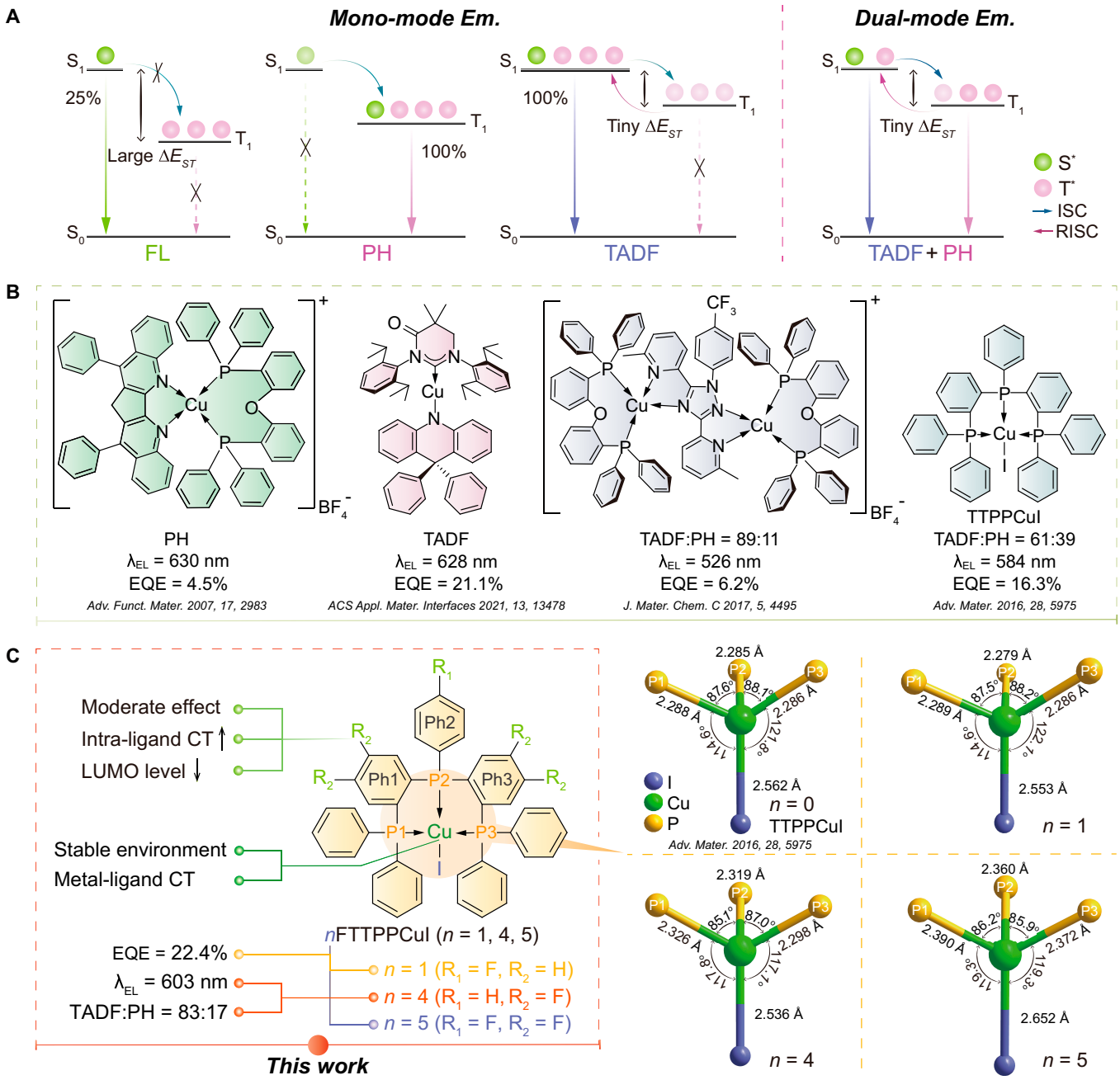


Fig. 1. Luminescence mechanism, design strategy, and molecular structures of copper complexes. (A) Electroluminescent (EL) mechanisms with various exciton harvesting processes. FL, PH, TADF, ISC, RISC, and ΔE_{ST} are the fluorescence, phosphorescence, thermally activated delayed fluorescence, intersystem crossing, reverse intersystem crossing, and singlet–triplet splitting energy, respectively. Green and pink balls denote singlet and triplet excitons, respectively. S_0, S_1, and T_1 states refer to the ground state, the first singlet, and triplet excited states, respectively. (B) Copper complexes featuring different TADF:PH ratios. λ is peak wavelength. EQE is external quantum efficiency. (C) Molecular design of *n*FTTPPCuI (*n* = 1, 4, and 5), and TTPPCuI (*n* = 0). Chemical structures of *n*FTTPPCuI (left), and their P–Cu–I core structures (right) are highlighted separately. Corresponding bond lengths and angles are marked. CT and SOC refer to charge transfer and spin-orbit coupling, respectively. LUMO is the lowest unoccupied molecular orbital.

levels and shifts the emission wavelength, making it difficult to simultaneously optimize both dual-emissive behavior and emission color [35].

Multinuclear copper cluster complexes, owing to their diverse channel emission, hold promise for applications in anti-counterfeiting, information encryption, and sensing, yet their structural complexity and challenging synthesis limit practical application [36–38]. By contrast, simple mononuclear dual-emissive copper complexes have been achieved in the blue and green regions [39–43], whereas achieving balanced dual emission in the red region remains challenging. Long-wavelength emission typically requires enhanced LCT or MLCT character to reduce the energy gap and red-shifted emission, which tends to suppress PH and favor TADF [44,45]. Additionally, smaller bandgaps are more prone to exciton thermal quenching and nonradiative decay, limiting emission efficiency [46–49]. Therefore, the development of efficient red dual-emissive copper complexes necessitates the precise optimization of intramolecular interactions. This, in turn, necessitates the development of ligand engineering strategies capable of modulating ligand-centered interactions.

For red-emitting copper complexes, most approaches rely on extending the π-conjugated ligand framework and enhancing molecular rigidity to achieve red-shifted emission and suppress nonradiative decay [50]. The first reported red-emitting mononuclear copper complex [Cu(mdpbq)(DPEphos)] (BF_4) primarily exhibited PH but suffered from limited exciton harvesting efficiency, yielding an external quantum efficiency (EQE) lower than 5% [51]. A subsequent development introduced a carbene–metal–amide-type copper complex, MAC*–Cu–DPAC, incorporating a strongly conjugated donor, 9,9-diphenyl-9,10-dihydroacridine (DPAC). This complex achieved red emission at ~630 nm with an EQE of ~20% [44]. However, the dominant ligand-centered excited state resulted in an almost zero ΔE_{ST} and RISC, leading to emission exclusively through TADF. As a result, PH was nearly completely suppressed, undermining the multifunctionality of dual-emissive behavior (Fig. 1B).

By contrast, inductive effects offer greater potential for the development of red dual-emissive materials. Electron-withdrawing groups, such as trifluoromethyl, can effectively modulate charge distribution and MLCT characteristics without markedly extending the π-conjugated system. This enables precise control over excited-state energy levels and emission mechanisms [52]. Although the resulting EQE remained relatively low (<10%) and the emission shift was modest (from 523 to 526 nm), the PH contribution increased to 11%, resulting in a more balanced emission profile (Fig. 1B). Compared with strategies based on π-conjugation extension, inductive effects provide broader advantages in tuning emission mechanisms, color, and excited-state dynamics, offering a promising design framework for high-performance red dual-emissive copper complexes.

Building on our previously reported yellow dual-emissive copper complex, TTPPCuI [12], this study introduces fluorine atoms with extremely small steric hindrance and suitable electron-withdrawing inductive effects into the tridentate triphosphine ligand (TTPP) [53,54]. Three fluorinated copper complexes, *n*FTTPPCuI ($n = 1$, 4, and 5), were synthesized (Fig. 1C, Figs. S1 to S22, and Scheme S1). In mononuclear copper complexes, the highest occupied molecular orbital (HOMO) is typically localized on the copper center, while the lowest unoccupied molecular orbital (LUMO) resides on the ligand framework [55–57]. Fluorine incorporation effectively lowers the LUMO energy, reducing the HOMO–LUMO energy gap and inducing red-shifted emission [58–60]. Moreover, because fluorine lacks π-conjugation, it does not substantially alter the nature of the emissive states, helping to maintain a balanced contribution from TADF and PH. Thus, 4FTTPPCuI represents the first long-wavelength copper complex to exhibit dual emission composed of ~80% TADF/~20% PH. FTTPPCuI exhibits a more balanced emission profile (~50% TADF/~50% PH), achieving an EQE of ~22% and a luminance of ~17,000 cd cm^{-2}. The emission wavelengths of the *n*FTTPPCuI series can be finely tuned within a narrow range of 574 to 603 nm, confirming the effectiveness of ligand engineering strategies in simultaneously regulating emission color and dual-emissive composition. These findings provide a viable pathway for the design of high-performance, long-wavelength dual-emissive copper complexes.

Results

Coordination structures and theoretical simulation

The tridentate phosphine ligands containing fluorine atoms form highly stable and rigid copper complexes, as confirmed by single-crystal structural analysis (Figs. S23, S35, and S36) [12,43,61–64]. In the *n*FTTPPCuI series, the overall tetrahedral coordination framework of the P–Cu–I core remains largely unchanged (Fig. 1C). However, stepwise fluorine substitution systematically modulates the local coordination environment and molecular geometry (Fig. S24 and Tables S1 to S4). In FTTPPCuI, the introduction of a single fluorine atom at the R_1 position of Ph2 (connected to the P2 atom) slightly reduces the electron-donating ability of the ligand, resulting in a marginal shortening of the Cu–I bond. In contrast, 4FTTPPCuI, with 4 fluorine atoms positioned at R_2 sites on Ph1 and Ph3, exhibits a stronger electron-withdrawing effect. This leads to a marked elongation of the P–Cu bond, while the Cu–I bond continues to shorten, suggesting an enhancement of metal–iodine interactions. Further fluorination in 5FTTPPCuI, through the addition of a fifth fluorine atom, causes excessive electron withdrawal from the metal center. This markedly alters the metal–ligand interaction mode. Both the P–Cu and C–P bonds are further elongated, increasing steric hindrance around the Cu^+ ion. As a result, the Cu–I bond is extended to 2.652 Å. Despite these changes, variation in bond angles is minimized, and the coordination geometry of 5FTTPPCuI closely approaches an ideal tetrahedral configuration. These observations confirm that fluorine substitution leads to distinct variations in coordination structures. Notably, no obvious intermolecular interactions are observed in 5FTTPPCuI due to its highly symmetrical ligand structure (Fig. S27). In contrast, the more distorted FTTPPCuI and 4FTTPPCuI exhibit weak hydrogen bonding interactions in the crystal lattice (Figs. S25 and S26).

Thermogravimetric analysis and differential scanning calorimetry reveal excellent thermal stability for all 3 complexes. The melting temperatures (T_m) exceed 310 °C, and decomposition temperatures (T_d) are higher than 340 °C. This high thermal resilience makes these complexes suitable candidates for vacuum-evaporated device fabrication (Fig. S28 and Table S8) [65].

The S_0 and excited singlet and triplet states were investigated using density functional theory (DFT) and time-dependent DFT (TDDFT) methods (Fig. 2A). The HOMOs of the 4 complexes are primarily localized on the CuI core and partially delocalized onto the nFTTPP segment, whereas the LUMOs are mainly distributed over the *o*-phenylene groups and the central phosphorus bridge of the nFTTPP ligands (Fig. S29). This spatial separation between the HOMOs and the LUMOs indicates pronounced charge-transfer interactions between the ligands and the CuI core. This separation effectively reduces the ΔE_{ST}, thereby creating favorable conditions for RISC from the T_1 to the S_1 excited state [66–68]. With increasing fluorine substitution, the LUMO energy levels are progressively lowered from −1.5 eV in TTPPCuI to −2.1 eV in 5FTTPPCuI. Concurrently, the HOMO–LUMO energy gap decreases from 3.3 eV (TTPPCuI) to 3.1 eV (5FTTPPCuI), consistent with the observed red-shifted emissions. This trend arises from the electron-withdrawing inductive effect of fluorine atoms, which weakens the MLCT and enhances the LCT component (Table S5) [69]. Experimental cyclic voltammetry (CV) measurements show HOMO and LUMO energy levels of approximately 5.5 and 2.9 eV, respectively, for the *n*FTTPPCuI complexes—well aligned with typical host and carrier-transporting materials (Fig. S32 and Table S8).

Natural transition orbital (NTO) analysis of the $S_0 \rightarrow S_1$ and the $S_0 \rightarrow T_1$ transitions reveals that the "holes" and "electrons" orbitals in both excited states are mainly localized on the CuI core and nFTTPP ligands, respectively, indicating that these excitations primarily correspond to HOMO→LUMO transitions

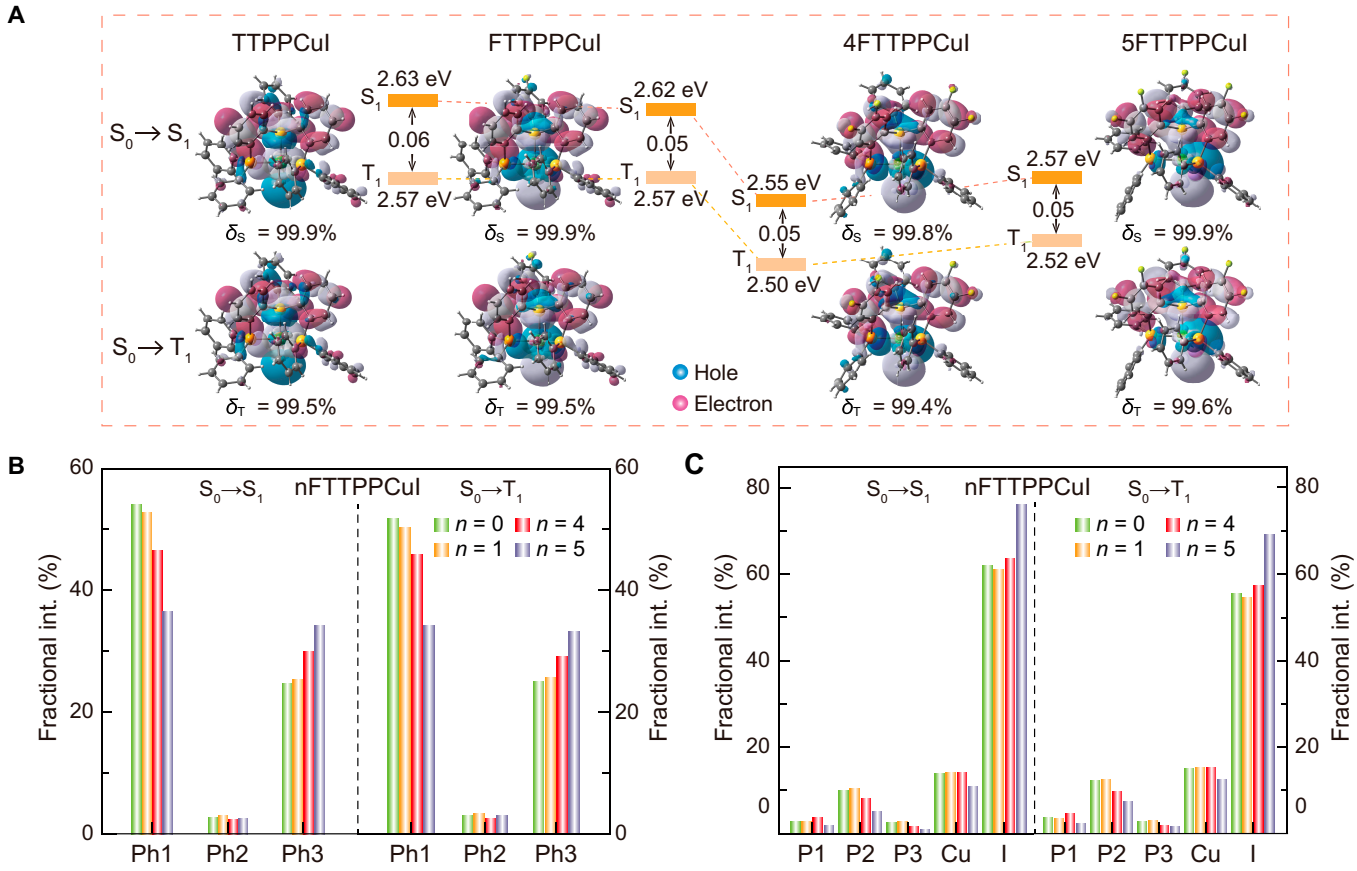


Fig. 2. Simulated electronic properties of *n*FTTPPCuI ($n = 0, 1, 4$, and 5) complexes. (A) Frontier molecular orbital (FMO) contours and key parameters of the $S_0 \rightarrow S_1$ and $S_0 \rightarrow T_1$ excitations simulated with natural transition orbital (NTO) analysis. The contours of "holes" and "electrons" are distinguished with blue and pink colors, respectively. δ and E represent the contribution weight and excited-state energy level, respectively. Subscripts "S" and "T" represent "singlet" and "triplet", respectively. (B) Contribution percentage of 3 phenyl rings (Ph1, Ph2, and Ph3) in *n*FTTPPCuI complexes to the electron during the $S_0 \rightarrow S_1$ and $S_0 \rightarrow T_1$ transitions. (C) Contribution percentage of representative atoms (P1, P2, P3, Cu, and I) to the hole during the $S_0 \rightarrow S_1$ and $S_0 \rightarrow T_1$ transitions.

with mixed M/ILCT characteristics. Fluorine substitution redistributes electron density within the ligands and enhances LCT characteristics (Fig. S30 and Tables S6 and S7).

In the $S_0 \rightarrow S_1$ transition of FTTPPCuI, the fluorine atom at the R_1 position of Ph3 induces only a weak inductive effect, resulting in marginal increases in the electron contributions from P2 and Ph2 by 0.25% and 0.38%, respectively (Fig. 2B and Fig. S31). In contrast, 4FTTPPCuI features fluorine atoms at the R_2 positions of Ph1 and Ph3, substantially enhancing the inductive effect. This modification drives electron density from the phenyl rings toward the central phosphorus atoms, increasing the electron contributions from P1 and P3 by 0.41% and 0.54%, respectively, while reducing that from Ph1 by 7.52%. The resulting excited-state reorganization strengthens the LCT character, lowers the LUMO energy level, narrows the HOMO–LUMO gap, and contributes to a more pronounced red shift [70]. In 5FTTPPCuI, an additional fluorine atom at the R_2 position of Ph2 works synergistically with the existing fluorine at the R_1 position. This induces a notable increase in the electron contribution from P2 by 5.57% and a modest increase from Ph2. Simultaneously, the contributions from P1 and Ph1 decrease markedly, resulting in strongly localized excited-state orbitals in the P2–Ph2 region. This increased asymmetry reduces charge separation, elevates the LUMO energy, and limits further red shifting. Moreover, the greater contribution of iodine to the hole orbitals in 5FTTPPCuI enhances ILCT character and diminishes MLCT, thereby increasing SOC and improving PH efficiency (Fig. 2C and Fig. S31) [71,72].

All 3 fluorinated complexes exhibit small ΔE_{ST} of approximately 0.05 eV (Table S8), which facilitate efficient intersystem crossing (ISC) and RISC between the S_1 and the T_1 states [73]. This enables dual emission and enhances EUE. Thus, fluorine-induced electron density redistribution not only alters excited-state configurations but also finely tunes the LUMO energy and overall bandgap, providing a mechanism for precise control of both emission wavelength and dual-emissive ratio.

Photophysical properties

The electronic absorption spectra of neat *n*FTTPPCuI films exhibit 4 absorption bands within the 200 to 500 nm range (Fig. 3A and Table S8). A strong absorption peak appears at ~240 nm, and a weaker band centered around 350 nm corresponds to $\pi \rightarrow \pi^*$ and $n \rightarrow \pi^*$ transitions, respectively. The absorption features near 370 nm are attributed to LCT, while the extended absorption tails from 400 to 500 nm are assigned to M/ILCT, similar to TTPPCuI (Fig. S33) [12]. Excitation spectra indicate multiple transition types—including LCT, MLCT, and ILCT—whose relative intensities vary among the complexes (Fig. 3A). Notably, 4FTTPPCuI displays the strongest excitation intensity at ~370 nm, indicating an enhanced LCT character. In contrast, LCT transitions in 5FTTPPCuI are reduced, while the excitation intensity near 400 nm is enhanced, pointing to an increased

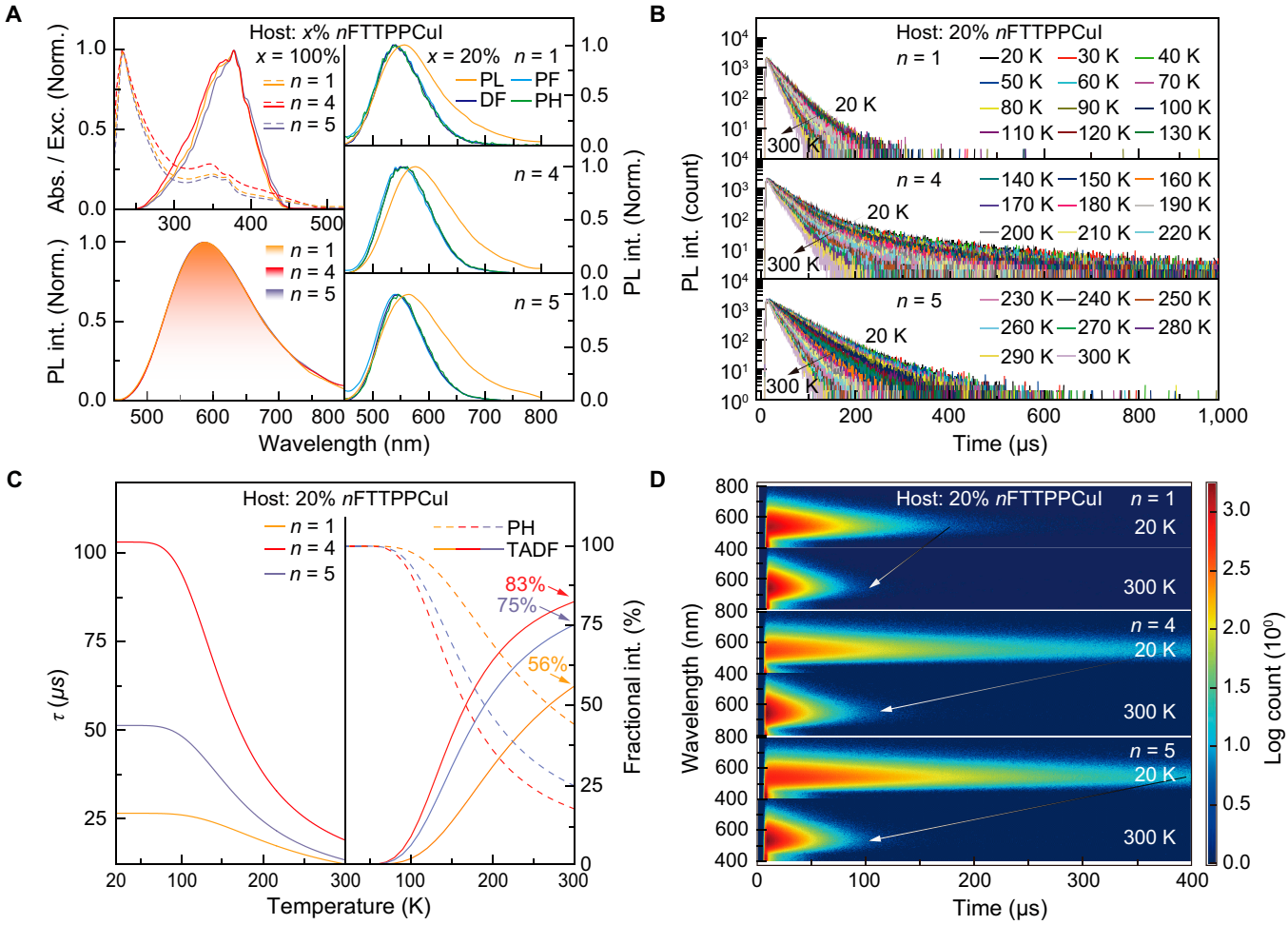


Fig. 3. Photophysical properties of *n*FTTPPCuI ($n = 1$, 4, and 5) complexes. (A) Electronic absorption spectra (dashed lines, upper left), excitation spectra (solid lines, upper left), and photoluminescence (PL) spectra (bottom left) of neat *n*FTTPPCuI films. PL, prompt fluorescence (PF), delayed fluorescence (DF), and PH spectra of Host:20% *n*FTTPPCuI-doped films (right). PF, DF, and PH spectra were measured with time-resolved technology, which recorded in the ranges of <1 μs, 1 to 200 μs, and >200 μs, respectively. (B) Temperature-dependent time decays for Host:20% *n*FTTPPCuI-doped films in the range of 20 to 300 K with an interval of 10 K. For $n = 1$, 4, and 5, the host materials are *m*CP, CBP, and *m*CP, respectively. The variation tendencies are marked with arrows. (C) Lifetime vs. temperature relationship (left) and temperature-dependent TADF:PH ratios (right) for doped films simulated with time decay data from (B). TADF fractional intensities at 300 K are marked. (D) Temperature-dependent time-resolved emission spectra (TRES) of doped films at 20 and 300 K. The variation tendencies are marked with arrows.

ILCT contribution. These trends are consistent with the excited-state compositions revealed by NTO analysis.

Compared with TTPPCuI, the photoluminescence (PL) spectra of neat *n*FTTPPCuI films show red-shifted emission by ~67 nm, with emission maxima near 590 nm at room temperature, and exhibit excellent photostability (Fig. 3A and Figs. S33 and S37) [25]. This red shift is attributed to fluorine-induced lowering of the LUMO energy, narrowing the HOMO–LUMO gap [60]. In solution, the PL spectra exhibit pronounced blue shifts in the emission wavelength, transitioning from approximately 590 nm in neat films to 410 nm. This notable blue shift can be attributed to a marked reduction in intermolecular interactions within the solution, which contrasts with the stronger interactions present in the films (Fig. S38). In doped films, PL emission peaks are observed at 555 nm for 1,3-bis(carbazol-9-yl)benzene (*m*CP):20% FTTPPCuI, 575 nm for 4,4′-bis(9H-carbazol-9-yl)biphenyl (CBP):20% 4FTTPPCuI, and 563 nm for *m*CP:20% 5FTTPPCuI (Fig. 3A and Fig. S44). These emissions show negligible temperature dependence, indicating a dual-emissive origin (Fig. S46) [74]. Furthermore, the prompt fluorescence (PF), delayed fluorescence (DF), and PH spectra of the doped films are nearly identical (Fig. 3A), suggesting similar electronic distributions and emission pathways for the S_1 and the T_1 states. From the PH and FL spectra of the neat films, the ΔE_{ST} for the *n*FTTPPCuI complexes are estimated to be ~0.04 eV, in agreement with theoretical values (Fig. S43). This small ΔE_{ST} facilitates efficient ISC and RISC, supporting the occurrence of dual emission.

Time decay curves of doped *n*FTTPPCuI films are bi-exponential, reflecting microsecond-scale lifetimes (Fig. 3B). At room temperature, these films exhibit shorter lifetimes (~20 μs) compared to their neat films (Figs. S34 and S45). In solution, lifetimes are further reduced due to increased nonradiative relaxation (Fig. S39). Furthermore, all 3 complexes exhibit high RISC rate constants (k_{RISC}), up to 10^5 s^{-1}, with quantum efficiencies of RISC (ϕ_{RISC}) reaching as high as 90% (Fig. S45 and Table S9). These findings suggest a transition from the T_1 to the S_1 excited state, thereby confirming the TADF behavior. Therefore, at 20 K, the excited state is predominantly confined to the T_1 state, resulting in PH emission characterized by a

relatively extended lifetime. As the temperature rises to 300 K, the excited state undergoes a thermally activated RISC process, transitioning from the long-lived T_1 state to the short-lived S_1 state, therefore decreasing the emission lifetime (Fig. 3B) [43,62,75].

Analysis of the dual-emissive components at 300 K shows that FTTPPCuI displays a balanced contribution from 56% TADF/44% PH (Fig. 3C). In contrast, 4FTTPPCuI exhibits a markedly enhanced TADF contribution (83%) due to its stronger LCT characteristics. In comparison, 5FTTPPCuI, owing to its more pronounced ILCT characteristics, shows an increased PH contribution, decreasing the TADF ratio to 75%. Consistent with these observations, the TADF/PH ratios measured in neat films exhibit the same trend as those in doped films (Figs. S40 and S41). This consistency confirms that the variations in TADF/PH ratios originate from the intrinsic excited-state compositions of the complexes rather than host–matrix effects. It is noteworthy that 4FTTPPCuI exhibits a relatively low k_{RISC} and the ratio of the singlet radiative to nonradiative rate constant (k_r^S / k_{nr}^S), resulting in a prolonged decay process and longer lifetime (Table S9). In comparison, 5FTTPPCuI shows a slight increase in the k_r^S / k_{nr}^S ratio, resulting in a modest reduction in its lifetime [20,65,72,76,77]. Additionally, temperature-dependent time-resolved emission spectra (TRES) show that, compared with neat films, the lifetimes in doped films are slightly prolonged due to suppression of nonradiative quenching by the host matrix (Fig. 3D and Figs. S42 and S47).

Electroluminescence properties

Vacuum-evaporated light-emitting devices with the configuration ITO|MoO_3 (6 nm)|TAPC (50 nm)|Host:*x*% *n*FTTPPCuI ($n = 0$, 1, 4, and 5) (20 nm)|TPBi (50 nm)|LiF (1 nm)|Al (100 nm) were fabricated. TAPC (di-[4-(N,N-ditolylamino) phenyl]cyclohexane) and TPBi (1,3,5-tris(N-phenylbenzimidazol-2-yl)benzene) served as the hole- and electron-transporting layers, respectively. *m*CP and CBP were used as the host materials (Fig. 4A and Fig. S51).

At optimized doping levels, the electroluminescent (EL) emission wavelengths were precisely tuned by varying the number of fluorine atoms in the ligand framework—from 572 nm (TTPPCuI) to 574 nm (FTTPPCuI), 584 nm (5FTTPPCuI), and 603 nm (4FTTPPCuI) (Fig. 4B). FTTPPCuI and 5FTTPPCuI both exhibited yellow EL emission, whereas 4FTTPPCuI exhibited a marked red shift (~30 nm), with corresponding Commission Internationale de l'Eclairage (CIE) coordinates of (0.58, 0.35) (Fig. 4C). Fluorine substitution also markedly improved electrical properties, reducing the turn-on voltage from 3.5 to 2.8 V (Figs. S52 to S61 and Tables S10 and S11), indicating enhanced carrier injection and recombination of 4FTTPPCuI [78]. Furthermore, the current–voltage characteristics of these devices were consistent with those of single-carrier transport devices based on *n*FTTPPCuI, confirming the important contribution of Cu(I) dopants to carrier transport (Fig. S62).

FTTPPCuI demonstrated the excellent device performance, achieving a peak EQE of ~22%, a current efficiency (CE) of ~64 cd A^{-1}, a power efficiency (PE) of ~63 lm W^{-1}, and a maximum luminance of ~17,000 cd m^{-2} (Fig. 4D and E). These values represent a ~6% improvement in EQE over TTPPCuI (Fig. S52) [12]. 5FTTPPCuI achieved an EQE of 14% and a peak luminance of ~7,000 cd m^{-2} (Fig. S55). Notably, 4FTTPPCuI produced red-shifted emission while retaining favorable device performance, with an EQE of 9%, a CE of ~20 cd A^{-1}, a PE of ~22 lm W^{-1}, and a maximum luminance of ~4,700 cd m^{-2} (Fig. S58). Moreover, 4FTTPPCuI was the first red-emitting copper complex to exhibit dual-emissive behavior and delivered better device performance in the red region with a CIE *x*-coordinate exceeding 0.56 (Fig. 4F), compared with other types of materials, such as perovskite emitters, highlighting its potential for red OLED applications [79,80]. Meanwhile, the PL quantum yield of 4FTTPPCuI (53%) was markedly lower than that of FTTPPCuI (88%) and 5FTTPPCuI (71%), consistent with its lower device EQE (Figs. S48 to S50). This suggests that the reduced efficiency arises from intrinsic emitter rather than device structure, highlighting the key role of emissive properties in device performance.

The exciton conversion dynamics in EL differ from those in PL. PL primarily excites the S_1 state, with the T_1 states generated through ISC, resulting in a limited population of triplet states. By contrast, EL directly forms approximately 75% T_1 excitons through carrier injection and recombination, serving as a more abundant source of triplets for the TADF process [81]. Although the EL spectra were temperature-independent, the emission lifetimes of *n*FTTPPCuI-based devices decreased by increasing temperature (Fig. 5A and Figs. S63 to S65). Among them, 4FTTPPCuI devices exhibited minimal temperature dependence in time-resolved decay, indicating a more efficient RISC process at low temperatures and a greater contribution from TADF.

Time-resolved electroluminescence emission spectra (TREES) showed that emissions from FTTPPCuI and 5FTTPPCuI devices were more temporally concentrated, whereas 4FTTPPCuI devices exhibited extended tails due to slower radiative decay (Fig. 5B). This behavior was attributed to stronger LCT character in 4FTTPPCuI, which reduced its T_1 energy level (2.50 eV) compared to FTTPPCuI (2.57 eV) and moved it further away from the triplet level of the *m*CP host (~2.9 eV) [82]. This alignment prolonged exciton lifetimes and extended the TREES tail. Sliced TREES further revealed that exciton confinement and recombination in 4FTTPPCuI were delayed by ~1 μs compared to FTTPPCuI. Unlike in PL, excited-state formation in the EL process is driven by charge injection, which further enhances charge-transfer characteristics [83]. FTTPPCuI-based devices exhibit lower TADF contributions and narrower emission bandwidths (~136 nm), while 4FTTPPCuI and 5FTTPPCuI devices show broader emission bands (~145 and ~140 nm, respectively) due to higher TADF components. These results underscore the importance of excited-state engineering in controlling EL behavior.

Discussion

"Ligand fluorination" strategy is adopted to rationally optimize the excited-state characteristics of CuI complexes for realizing efficient red dual emission. The feature of fluorine atom with only electron-withdrawing inductive effect is utilized to continuously adjust the emission wavelengths of *n*FTTPPCuI complexes in a range from 574 to 603 nm by changing the substitution position and number of fluorine atoms. Simultaneously, the modulated MLCT by fluorination makes TADF/PH ratios varied from 56/44 to 83/17. FTTPPCuI with a balanced TADF/PH ratio of ~50/50 endowed its device with the EQE up to ~22%, while 4FTTPPCuI-based devices achieved the desired red emission purity with CIE_x beyond 0.56, demonstrating the first red dual-emissive OLED. This work demonstrates not only the feasibility of controllable excited-state optimization by single electronic

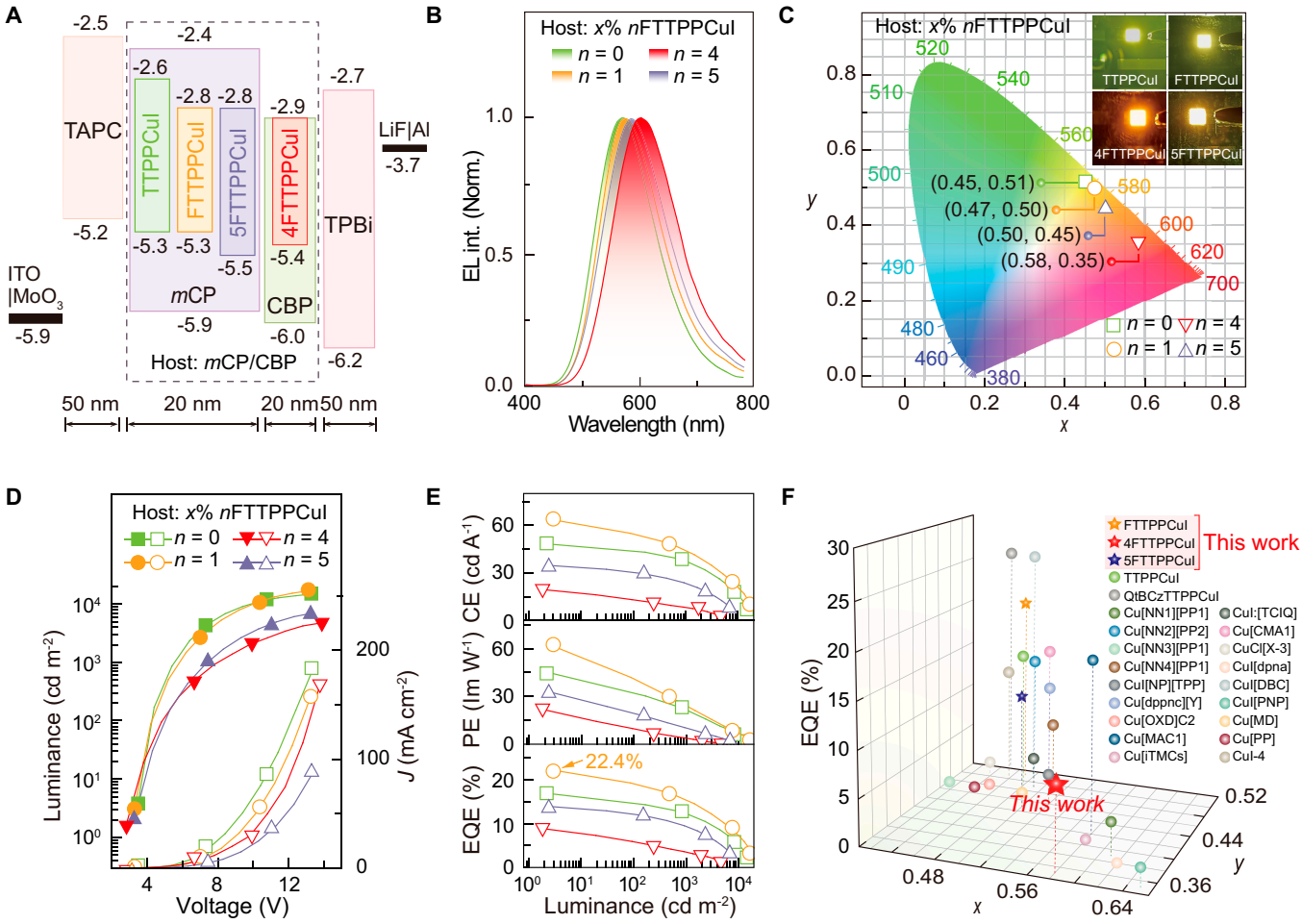


Fig. 4. EL performance of *n*FTTPPCuI (*n* = 0, 1, 4, and 5)-based OLEDs. (A) Energy level diagram of the devices. (B) EL spectra at the respective optimal doping concentrations. (C) Device photos (inset) at 5 V, and the corresponding chromatic coordinates at CIE 1931 panel. CIE coordinates at the respective optimal doping concentrations are marked. (D) Current density (*J*, open symbols)–luminance (solid symbols)–voltage characteristics of the devices at the optimal doping concentrations (*x*%). (E) Efficiencies vs. luminance relationships of the devices. CE and PE refer to current and power efficiencies, respectively. EQE value of FTTPPCuI at the maximum are marked with an arrow. (F) Milestones of the EQE values and the corresponding chromatic coordinates at CIE achieved by copper complexes with EL wavelengths in the long-wavelength range in devices. The corresponding detailed performances are listed in Table S12. The 4FTTPPCuI complex is highlighted with a red pentagram, representing the first red-emitting copper complex exhibiting dual-emissive behavior.

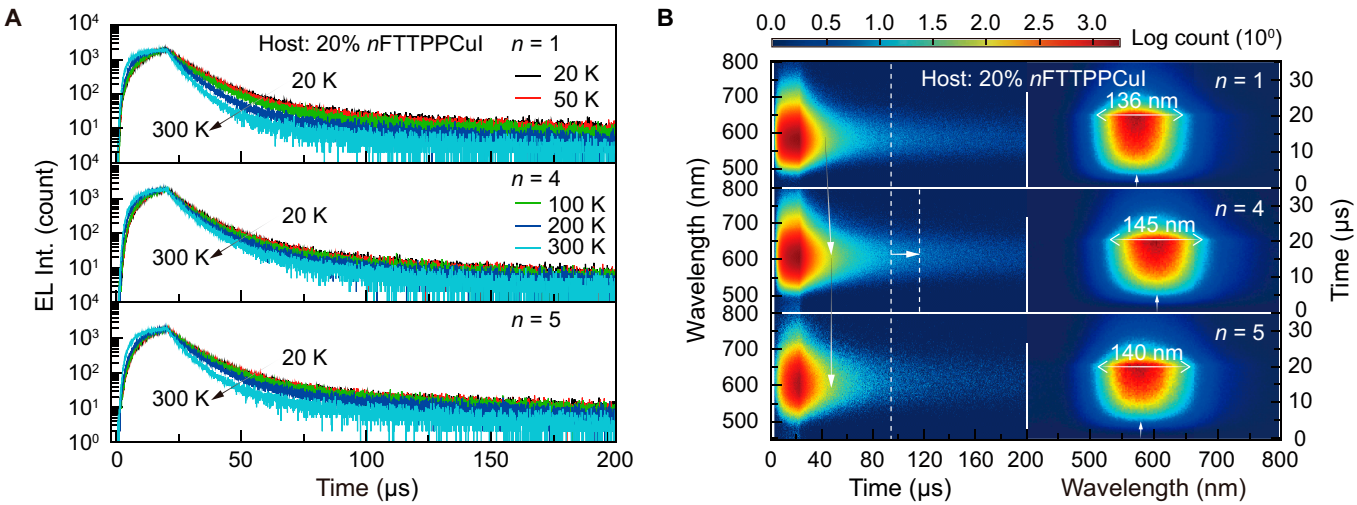


Fig. 5. Exciton kinetics in the devices. (A) EL time decays of Host:20% *n*FTTPPCuI (*n* = 1, 4, and 5)-based devices in the temperature range of 20 to 300 K. (B) Contours of time-resolved electroluminescence emission spectra (TREES, left) in the range of 200 μs and sliced contours (right) of the OLEDs at the first 35 μs. Recombination ranges are at the first 20 μs.

effects, but also the potential of dual-emissive systems for practical display and lighting applications.

Materials and Methods

Experimental details, thermal properties, DFT simulation, electrochemical and photophysical properties, and device performance are included in the Supplementary Materials.

Acknowledgments

Funding: This work was supported by the National Natural Science Foundation of China (22375057, W2412073, 52273173, 22325502, 92461304, and 22305073), the Natural Science Foundation of Heilongjiang Province (PL2024B014 and YQ2022B010), and the Education Department of Heilongjiang Province (2024-KYYWF-0123).

Author contributions: X.L.: Writing—review and editing, writing—original draft, validation, methodology, data curation, and conceptualization. G.C.: Methodology and investigation. C.L.: Methodology and investigation. J.H.: Validation and resources. J.N.: Supervision and software. C.D.: Supervision, software, and resources. C.H.: Supervision, software, resources, and formal analysis. J.Z.: Writing—review and editing, writing—original draft, methodology, funding acquisition, data curation, and conceptualization. A.A.K.: Conceptualization and supervision. H.X.: Writing—review and editing, writing—original draft, visualization, validation, supervision, software, resources, project administration, methodology, investigation, funding acquisition, formal analysis, data curation, and conceptualization.

Competing interests: The authors declare that they have no competing interests.

Data Availability

All data supporting the findings of this study are presented in the article and the Supplementary Materials. Additional data are available from the corresponding authors upon reasonable request.

Supplementary Materials

Figs. S1 to S65
Tables S1 to S12

References

1. Mao M, Li HY, Lo KW, Zhang DD, Duan L, Xu S, Wan QY, Tan KX, An PC, Cheng G, et al. Color-tunable organic light-emitting diodes with single Pt (O^N^C^N)-dibenzofuran emitter exhibiting high external quantum efficiency of ≈30% and superior operational lifetime. *Adv Mater*. 2024;36(25):2311020.
2. Ge LS, Zhang W, Hao YH, Li M, Liu Y, Zhou M, Cui LS. Efficient and stable narrowband pure-red light-emitting diodes with electroluminescence efficiencies exceeding 43%. *J Am Chem Soc*. 2024;146(47):32826–32836.
3. Zou Y, Hu JH, Yu MX, Miao JS, Xie ZY, Qiu YT, Cao XS, Yang CL. High-performance narrowband pure-red OLEDs with external quantum efficiencies up to 36.1% and ultralow efficiency roll-off. *Adv Mater*. 2022;34(29):Article 2201442.
4. Li XN, Xie YJ, Li Z. Diversity of luminescent metal complexes in OLEDs: Beyond traditional precious metals. *Chem Asian J*. 2021;16(19):2817–2829.
5. Hong G, Gan XM, Leonhardt C, Zhang Z, Seibert J, Busch JM, Bräse S. A brief history of OLEDs-emitter development and industry milestones. *Adv Mater*. 2021;33(9):2005630.
6. Zhang XJ, Xu H. Electroluminescent clusters. *Angew Chem Int Ed*. 2024;63(10):Article e202317597.
7. Zhang C, Zhang DD, Bin ZY, Liu ZY, Zhang YW, Lee H, Kwon JH, Duan L. Color-tunable all-fluorescent white organic light-emitting diodes with a high external quantum efficiency over 30% and extended device lifetime. *Adv Mater*. 2022;34(22):2103102.
8. Zhang CH, Zhao YS. Flexible photonic materials and devices: Synthetic strategies, sensing properties, and wearable applications. *Adv Mater*. 2025;37(49):Article 2415856.
9. Mojumder MRH, Kim S, Yu CJ. Soft artificial synapse electronics. *Research*. 2025;8:0582.
10. Zhang DD, Huang TY, Duan L. Emerging self-emissive technologies for flexible displays. *Adv Mater*. 2020;32(15):1902391.
11. Su RT, Park SH, Ouyang X, Ahn SI, McAlpine MC. 3D-printed flexible organic light-emitting diode displays. *Sci Adv*. 2022;8(1):Article eabl8798.
12. Zhang J, Duan CB, Han CM, Yang H, Wei Y, Xu H. Balanced dual emissions from tridentate phosphine-coordinate copper(I) complexes toward highly efficient yellow OLEDs. *Adv Mater*. 2016;28(28):5975–5979.
13. Helfrich W, Schneider WG. Transients of volume-controlled current and of recombination radiation in anthracene. *J Chem Phys*. 1966;44(8):2902–2909.
14. Sheats JR, Antoniadis H, Hueschen M, Leonard W, Miller J, Moon R, Roitman D, Stocking A. Organic electroluminescent devices. *Science*. 1996;273(5277):884–888.
15. Baldo MA, O'Brien DF, You Y, Shoustikov A, Sibley S, Thompson ME, Forrest SR. Highly efficient phosphorescent emission from organic electroluminescent devices. *Nature*. 1998;395(6698):151–154.
16. Uoyama H, Goushi K, Shizu K, Nomura H, Adachi C. Highly efficient organic light-emitting diodes from delayed fluorescence. *Nature*. 2012;492(7428):234–238.
17. Zhang Y, Forrest SR. Triplets contribute to both an increase and loss in fluorescent yield in organic light emitting diodes. *Phys Rev Lett*. 2012;108(26):Article 267404.
18. Baldo MA, Adachi C, Forrest SR. Transient analysis of organic electrophosphorescence. II. Transient analysis of triplet-triplet annihilation. *Phys Rev B*. 2000;62(16):10967–10977.
19. Leitl MJ, Krylova VA, Djurovich PI, Thompson ME, Yersin H. Phosphorescence versus thermally activated delayed fluorescence. Controlling singlet-triplet splitting in brightly emitting and sublimable cu(I), compounds. *J Am Chem Soc*. 2014;136(45):16032–16038.
20. Hofbeck T, Monkowius U, Yersin H. Highly efficient luminescence of cu(I) compounds: Thermally activated delayed fluorescence combined with short-lived phosphorescence. *J Am Chem Soc*. 2015;137(1):399–404.
21. Zhu ZQ, Fleetham T, Turner E, Li J. Harvesting all electrogenerated excitons through metal assisted delayed fluorescent materials. *Adv Mater*. 2015;27(15):2533–2537.
22. Chen XL, Yu RM, Wu XY, Liang D, Jia JH, Lu CZ. A strongly greenish-blue-emitting Cu_4Cl_4 cluster with an efficient spin-orbit coupling (SOC): Fast phosphorescence versus

thermally activated delayed fluorescence. *Chem Commun*. 2016;52(37):6288–6291.
23. Xie MC, Han CM, Zhang J, Xie GH, Xu H. White electroluminescent phosphine-chelated copper iodide nanoclusters. *Chem Mater*. 2017;29(16):6606–6610.
24. Duan CB, Han CM, Du RM, Wei Y, Xu H. High-efficiency blue dual-emissive exciplex boosts full-radiative white electroluminescence. *Adv Optical Mater*. 2018;6(19):1800437.
25. Xie MC, Han CM, Liang QQ, Zhang J, Xie GH, Xu H. Highly efficient sky blue electroluminescence from ligand-activated copper iodide clusters: Overcoming the limitations of cluster light-emitting diodes. *Sci Adv*. 2019;5(6):eaav9857.
26. Baranov AY, Berezin AS, Samsonenko DG, Mazur AS, Tolstoy PM, Plyusnin VF, Kolesnikov IE, Artem'ev AV. New Cu(I) halide complexes showing TADF combined with room temperature phosphorescence: The balance tuned by halogens. *Dalton Trans*. 2020;49(10):3155–3163.
27. Yersin H, Monkowius U. Thermally activated delayed fluorescence and beyond. Photophysics and material design strategies. *Adv Photonics Res*. 2024;6(8):Article 2400111.
28. Liu YR, Yiu SC, Ho CL, Wong WY. Recent advances in copper complexes for electrical/light energy conversion. *Coord Chem Rev*. 2018;375:514–557.
29. Li Y, Xu SW, Zhang XF, Man Y, Zhang J, Zhang GM, Chen S, Duan CB, Han CM, Xu H. Bulk passivation enables hundredfold-enhanced electroluminescence of monophosphine Cu_4I_4 cubes. *Angew Chem Int Ed*. 2023;62(39):Article e202308410.
30. Sun JN, Li NY, Gong ZK, Man Y, Zhong CL, Duan CB, Chen S, Zhang J, Han CM, Xu H. Ligand-mediate exciton allocation enables efficient cluster-based white light-emitting diodes via single and heavy doping. *Nat Commun*. 2024;15(1):4997.
31. Housecroft CE, Constable EC. TADF: Enabling luminescent copper(I) coordination compounds for light-emitting electrochemical cells. *J Mater Chem C*. 2022;10(12):4456–4482.
32. Lüdtke N, Föller J, Marian CM. Understanding the luminescence properties of cu(I) complexes: A quantum chemical perusal. *PhysChemChemPhys*. 2020;22(41):23530–23544.
33. Czerwieniec R, Leitl MJ, Homeier HH, Yersin H. Cu(I) complexes-thermally activated delayed fluorescence. Photophysical approach and material design. *Coord Chem Rev*. 2016;325:2–28.
34. Zhang XW, Huang CH, Yang MX, Chen XL, Lu CZ. Rotational isomerization: Spontaneous structural transformation of a thermally activated delayed fluorescence binuclear copper(I) complex. *Dalton Trans*. 2023;52(29):9893–9898.
35. Li TY, Zheng SJ, Djurovich PI, Thompson ME. Two-coordinate thermally activated delayed fluorescence coinage metal complexes: Molecular design, photophysical characters, and device application. *Chem Rev*. 2024;124(7):4332–4392.
36. Forni A, Malpicci D, Lucenti E, Zecchinello L, Colombo A, Cariati E. Recent advances in mono- and multi-nuclear photoluminescent Cu(I) complexes with nitrogen containing ligands and their stimuli responsiveness. *Chem Sci*. 2025;16(44):20755–20805.
37. Musina EI, Strelnik ID, Yakhya VA, Spiridonova YS, Litvinov IA, Shmelev AG, Zueva EM, Khrizanforov MN, Gao F, Xu H, et al. Luminescent copper(I) heteroleptic complexes based on BiPy and bulky diphosphine ligands. *Dyes Pigments*. 2026;246:Article 113374.
38. Strelnik ID, Kolesnikov IE, Kalinichev AA, Gerasimova TP, Akhmadgaleev KD, Dayanova IR, Karasik AA. Is dual emission of copper subgroup d_{10}-metal complexes a necessary and sufficient condition for ratiometric luminescence thermometry? *Mendeleev Commun*. 2024;34(4):457–471.
39. Zhang FL, Guan YQ, Chen XL, Wang SS, Liang D, Feng YF, Chen SF, Li SZ, Li ZY, Zhang FQ, et al. Syntheses, photoluminescence, and electroluminescence of a series of Sublimable bipolar cationic cuprous complexes with thermally activated delayed fluorescence. *Inorg Chem*. 2017;56(7):3742–3753.
40. Li XY, Zhang JY, Zhao ZF, Yu X, Li PC, Yao Y, Liu ZW, Jin QH, Bian ZQ, Lu ZH, et al. Bluish-green Cu(I)dimers chelated with thiophene ring-introduced diphosphine ligands for both singlet and triplet harvesting in OLEDs. *ACS Appl Mater*. 2019;11(3):3262–3270.
41. Artem'ev AV, Demyanov YV, Rakhmanova MI, Bagryanskaya IY. Pyridylarsine-based Cu(I) complexes showing TADF mixed with fast phosphorescence: A speeding-up emission rate using arsine ligands. *Dalton Trans*. 2022;51(3):1048–1055.
42. Zhao ZK, He TF, Gao Q, Ren AM, Wu TS, Guo JF, Chu HY, Su ZM, Li H, Zou LY. Theoretical investigation and molecular design: A series of tripod-type Cu(I) blue light thermally activated delayed fluorescence materials. *Inorg Chem*. 2024;63(38):17435–17448.
43. Jiang JX, Zhao YF, Li ZJ, Ye YXY, Wu ZY, Jiang FL, Chen L, Hong MC. Cu(I) halide complex featuring blue thermally activated delayed fluorescence and aggregate induced emission for efficient X-ray scintillation and imaging. *Angew Chem Int Ed*. 2025;64(18):Article e202422995.
44. Ying A, Huang YH, Lu CH, Chen ZX, Lee WK, Zeng X, Chen TH, Cao XS, Wu CC, Gong SL, et al. High-efficiency red electroluminescence based on a carbene-Cu(I)-acridine complex. *ACS Appl Mater Interfaces*. 2021;13(11):13478–13486.
45. Gernert M, Wolf LB, Kerner F, Müller U, Schmiedel A, Holzapfel M, Marian CM, Pflaum J, Lambert C, Steffen A. Cyclic (amino)(aryl)carbenes enter the field of chromophore ligands: Expanded π system leads to unusually deep red emitting CuI compounds. *J Am Chem Soc*. 2020;142(19):8897–8909.
46. Yang H, Zheng J, Xie M, Luo D, Tang WJ, Peng SK, Cheng G, Zhang XJ, Zhou XP, Che CM, et al. Aggregation-enhanced emission in a red Cu(I) emitter with quantum yield >99%. *ACS Materials Lett*. 2022;4(10):1921–1928.
47. Wei YC, Wang SF, Hu Y, Liao LS, Chen DG, Chang KH, Wang CW, Liu SH, Chan WH, Liao JL, et al. Overcoming the energy gap law in near-infrared OLEDs by exciton-vibration decoupling. *Nat Photonics*. 2020;14(9):570–577.
48. Kim JH, Yun JH, Lee JY. Recent progress of highly efficient red and near-infrared thermally activated delayed fluorescent emitters. *Adv Optical Mater*. 2018;6(18):1800255.
49. Caspar JV, Meyer TJ. Application of the energy gap law to nonradiative, excited-state decay. *J Phys Chem*. 1983;87(6):952–957.
50. Zampetti A, Minotto A, Cacialli F. Near-infrared (NIR) organic light-emitting diodes (OLEDs): Challenges and opportunities. *Adv Funct Mater*. 2019;29(21):1807623.
51. Zhang QS, Ding JQ, Cheng YX, Wang LX, Xie ZY, Jing XB, Wang FS. Novel heteroleptic CuI complexes with tunable emission color for efficient phosphorescent light-emitting diodes. *Adv Funct Mater*. 2007;17(15):2983–2990.

52. Lin L, Chen DH, Yu RM, Chen XL, Zhu WJ, Liang D, Chang JF, Zhang Q, Lu CZ. Photo- and electro-luminescence of three TADF binuclear Cu(I) complexes with functional tetraimine ligands. *J Mater Chem C*. 2017;5(18):4495–4504.
53. Busch JM, Zink DM, Di Martino-Fumo P, Rehak FR, Boden P, Steiger S, Fuhr O, Nieger M, Klopper W, Gerhards M, et al. Highly soluble fluorine containing Cu(I) AlkylPyrPhos TADF complexes. *Dalton Trans*. 2019;48(41):15687–15698.
54. Müller K, Faeh C, Diederich F. Fluorine in pharmaceuticals: Looking beyond intuition. *Science*. 2007;317(5846):1881–1886.
55. Klein M, Rau N, Wende M, Sundermeyer J, Cheng G, Che CM, Schinabeck A, Yersin H. Cu(I) and ag(I) complexes with a new type of rigid tridentate N, P, P-ligand for thermally activated delayed fluorescence and OLEDs with high external quantum efficiency. *Chem Mater*. 2020;32(24):10365–10382.
56. Shimoji H, Kihara H, Sumida A, Imoto H, Naka K. Synthesis of phosphorus/arsenic tridentate ligands and their application for luminescent copper(I) halide complexes. *Eur J Inorg Chem*. 2024;27(19):Article e202400090.
57. Liu YL, Zhu RQ, Liu L, Zhong XX, Li FB, Zhou GJ, Qin HM. Highly efficient TADF-OLEDs with copper(I) halide complexes containing unsymmetrically substituted thiophenyl triphosphine. *Inorg Chem Front*. 2025;12:1139–1155.
58. Jing YM, Wang FZ, Zheng YX, Zuo JL. Efficient deep red electroluminescence of iridium(III) complexes with 2,3-diphenylquinoxaline derivatives and tetraphenylimidodiphosphinate. *J Mater Chem C*. 2017;5(15):3714–3724.
59. Liu SN, Tong KN, Zhao Y, Cheng JF, Fung MK, Fan J. Efficient red phosphorescent Ir(III) complexes based on rigid ligands with high external quantum efficiency and low efficiency roll-off. *J Mater Chem C*. 2020;8(18):6168–6175.
60. Igawa S, Hashimoto M, Kawata I, Yashima M, Hoshino M, Osawa M. Highly efficient green organic light-emitting diodes containing luminescent tetrahedral copper(I) complexes. *J Mater Chem C*. 2013;1(3):542–551.
61. Fukuma S, Fu J, Nakamuro T, Shang R, Nakamura E. Deep-red emitting copper(I) indenediyltrisphosphine complexes with minimized skeletal vibrations and configurational disorder. *Angew Chem Int Ed*. 2024;64(4):Article e202416583.
62. Niu JX, Gao FF, Wang Y, Lu W, Zhang J, He JX, Lou XJ, Ma YX, Duan CB, Han CM, et al. Equalized dual emissions from copper complexes via multichannel balanced intersystem crossing: Towards 100% quantum efficiencies. *Angew Chem Int Ed*. 2025;64(28):Article e202508667.
63. Yu XL, Ryadun AA, Pavlov DI, Guselnikova TY, Potapov AS, Fedin VP. Ln-MOF-based hydrogel films with tunable luminescence and afterglow behavior for visual detection of ofloxacin and anti-counterfeiting applications. *Adv Mater*. 2024;36(19):2311939.
64. Jin Y, Peng QC, Xie JW, Li K, Zang SQ. Photo-activated circularly polarized luminescence film based on aggregation-induced emission copper(I) cluster-assembled materials. *Angew Chem Int Ed*. 2023;62(19):Article e202301000.
65. Ying A, Tan Y, Gong SL. Highly efficient copper(I) emitters supported by secondary metal-ligand interactions. *Adv Optical Mater*. 2024;12(17):2303333.
66. Tang R, Xu S, Cheng G, Low KH, Zhang DD, Duan L, Che CM. Highly stable and efficient copper(I) sensitizer for narrowband red organic light-emitting diodes with an operational lifetime (LT95) of up to 3689 h at 1000 cd m^{-2}. *Nat Commun*. 2025;16(1):7776.
67. Zobel JP, Wernbacher AM, González L. Efficient reverse intersystem crossing in carbene-copper-amide TADF emitters via an intermediate triplet state. *Angew Chem Int Ed*. 2023;62(15):Article e202217620.
68. Wang HJ, Liu Y, Yu BQ, Song SQ, Zheng YX, Liu KL, Chen PK, Wang HL, Jiang JZ, Li TY. A configurationally confined thermally activated delayed fluorescent two-coordinate CuI complex for efficient blue electroluminescence. *Angew Chem Int Ed*. 2023;62(7): Article e202217195.
69. Zhang YW, Zhang DD, Wei JB, Liu ZY, Lu Y, Duan L. Multi-resonance induced thermally activated delayed fluorophores for narrowband green OLEDs. *Angew Chem Int Ed*. 2019;58(47):16912–16917.
70. Kothavale S, Chung WJ, Lee JY. Rational molecular design of highly efficient yellow-red thermally activated delayed fluorescent emitters: A combined effect of auxiliary fluorine and rigidified acceptor unit. *ACS Appl Mater Interfaces*. 2020;12(16):18730–18738.
71. Garain S, Ansari SN, Kongasseri AA, Chandra Garain B, Pati SK, George SJ. Room temperature charge-transfer phosphorescence from organic donor-acceptor co-crystals. *Chem Sci*. 2022;13(34):10011–10019.
72. Farokhi A, Lipinski S, Cavinato LM, Shahroosvand H, Pashaei B, Karimi S, Bellani S, Bonaccorso F, Costa RD. Metal complex-based TADF: Design, characterization, and lighting devices. *Chem Soc Rev*. 2025;54:266–340.
73. Wang X, Niu GW, Zhou ZX, Song ZC, Qin K, Yao XK, Yang ZJ, Wang XZ, Wang H, Liu Z, et al. Halogenated thermally activated delayed fluorescence materials for efficient scintillation. *Research*. 2023;6:0090.
74. Wang ZQ, Sun XJ, Fu WJ, Xu C, Ji BM. Four-coordinate cu(I) complexes supported by N-heterocyclic carbene ligands bearing electron-donating/withdrawing groups: Synthesis, structures and photophysical properties. *J Lumin*. 2018;204:618–625.
75. Hamze R, Peltier JL, Sylvinson D, Jung M, Cardenas J, Haiges R, Soleilhavoup M, Jazzar R, Djurovich PI, Bertrand G, et al. Eliminating nonradiative decay in cu(I) emitters: >99% quantum efficiency and microsecond lifetime. *Science*. 2019;363(6427):601–606.
76. Huang ZY, Xie HH, Miao JS, Wei YX, Zou Y, Hua T, Cao XS, Yang CL. Charge transfer excited state promoted multiple resonance delayed fluorescence emitter for high-performance narrowband electroluminescence. *J Am Chem Soc*. 2023;145(23):12550–12560.
77. Ochi J, Yamasaki Y, Tanaka K, Kondo Y, Isayama K, Oda S, Kondo M, Hatakeyama T. Highly efficient multi-resonance thermally activated delayed fluorescence material toward a BT.2020 deep-blue emitter. *Nat Commun*. 2024;15(1): Article 2361.
78. Zhang DH, Jiang SS, Tao XD, Lin FL, Meng LY, Chen XL, Lu CZ. Efficient spin-flip between charge-transfer states for high-performance electroluminescence, without an intermediate locally excited state. *Research*. 2023;6:0155.
79. Li YJ, Meng N, Xu YT, Yu BF, Liu JH, Cui YH, Wang ZQ, Ke XW, Pan TF, Min X, et al. Sequential layer-by-layer deposition for high-performance fully thermal-evaporated red perovskite light-emitting diodes. *Nat Commun*. 2025;16(1):6908.
80. Liu N, Liu ZZ, Huang YL, Du PP, Zhang X, Leng YX, Luo JJ, Du J, Tang J. Fluorine-modified passivator for efficient

vacuum-deposited pure-red perovskite light-emitting diodes. *Light Sci Appl*. 2025;14(1):118.
81. Shizu K, Lee J, Tanaka H, Nomura H, Yasuda T, Kaji H, Adachi C. Highly efficient electroluminescence from purely organic donor-acceptor systems. *Pure Appl Chem*. 2015;87(7):627–638.
82. Öner S, Kuila S, Stavrou K, Danos A, Fox MA, Monkman AP, Bryce MR. Exciplex, not heavy-atom effect, controls the triplet dynamics of a series of sulfur-containing thermally activated delayed fluorescence molecules. *Chem Mater*. 2024;36(15):7135–7150.
83. Miranda Salinas H, Hung YT, Chen YS, Luo D, Kao HC, Chang CH, Wong KT, Monkman A. Controlling through-space and through-bond intramolecular charge transfer in bridged D-D-A TADF emitters. *J Mater Chem C*. 2021;9(28):8819–8833.